Erratum: "Nonlinear excitations in electron-positron-ion plasmas in accretion disks of active galactic nuclei" [Phys. Plasmas 14, 102901 (2007)]

W. M. Moslem[1]

Institut für Theoretische Physik IV,

Fakultät für Physik und Astronomie,

Ruhr-Universität Bochum, D-44780 Bochum, Germany and and

Department of Physics, Faculty of Education-Port Said, Suez Canal University, Egypt

I. Kourakis[2]

Centre for Plasma Physics, Department of Physics and Astronomy,

Queen's University Belfast, BT7 1 NN Northern Ireland

P. K. Shukla[3]

Institut für Theoretische Physik IV,

Fakultät für Physik und Astronomie,

Ruhr-Universität Bochum, D-44780 Bochum,

Germany; School of Physics, University of Kwazulu-Natal,

Natal 4000, South Africa; Department of Physics,

Umeå University, SE-90187 Umeå,

Sweden; Max-Planck Institut für Extraterrestrische Physik,

D-85741 Garching, Germany; GoLP/Instituto Superior Técnico,

1049-001 Lisbon, Portugal; CCLRC Centre for Fundamental Physics,

Rutherford Appleton Laboratory, Chilton, Didcot,

Oxon 0X11 0QX, UK; SUPA Department of Physics,

University of Strathclyde, Glasgow G 40NG, UK.

R. Schlickeiser[4]

Institut für Theoretische Physik IV,

Fakultät für Physik und Astronomie,

Ruhr-Universität Bochum, D-44780 Bochum, Germany

An algebraic calculation error has been introduced in the form of the coefficients A, B and C – appearing in Eqs. (17) and (28) in Ref. 1 – as they were defined in expressions (18), (19) and (29) therein, respectively. Although the qualitative aspects of the original article remain valid, and so does the overall methodology of the paper, the error has inevitably affected the numerical evaluation (of A, B and C) leading to the graphic representation of relevant quantities and, consequently, the parametric study which relied on them. The layout of Figs. 5 - 7 and their captions also contained errors, regretfully. The purpose of this Erratum is to provide the complete set of exact analytical expressions for the coefficients and also to present the plots in their correct form. A brief comment on the modifications occurring in the plots is also provided below, where appropriate.

The correct expressions for the coefficients read

$$A = B\left[\frac{3\lambda^2\delta}{(\lambda^2 - 2\sigma_p\delta)^3} - \frac{3\lambda^2}{(\lambda^2-2)^3} + \beta\sigma_i^2\right], \tag{1}$$

$$B = \left[\frac{2\lambda\delta}{(\lambda^2 - 2\sigma_p\delta)^2} + \frac{2\lambda}{(\lambda^2-2)^2}\right]^{-1}, \tag{2}$$

and

$$C = \frac{3}{2}B\left[\frac{\lambda^2\delta(5\lambda^2 + 8\sigma_p\delta)}{(\lambda^2 - 2\sigma_p\delta)^5} + \frac{\lambda^2(5\lambda^2+8)}{(\lambda^2-2)^5} - \frac{1}{3}\beta\sigma_i^3\right]. \tag{3}$$

A brief discussion of the amended figures is presented in the following. The behavior of the amplitude ϕ_0 and width W of the solitary potential excitations is depicted in Figs. 1 and 2. The qualitative profile is as described in Ref. 1, although the values predicted for the pulse excitation amplitude (width) turn out to be larger (smaller).

Recall that, according to the assumptions in Section IV of Ref. 1, referring to critical plasma compositions where quadratic nonlinearity may be negligible (so resorting to higher-order nonlinearity is necessary), we need to determine the parameter region (in terms of the propagation speed λ) where A is of the order of ε while Δ is positive. This region is identified with the help of Figs. 3 - 5 [referring to parts (a) and (b) therein], for different values of the positron-to-electron density ratio δ and of the electron-to-ion temperature ratio σ_i, while the corresponding strength of the cubic nonlinearity coefficient C is shown in part (c) in those plots. It is seen (Fig. 3a) that for a small value of $\delta = 0.1$ (i.e. for high concentration of fixed ions), the range of permitted λ values is very narrow (essentially in the vicinity of $\lambda \approx 2.5$ – highly supersonic pulses are thus predicted) for both values of σ_i considered (cf. the solid and dashed curves in the plots). By increasing δ to 0.5 (Fig. 4) and 0.9 (Fig.

5), the region of permitted values of λ is slightly enlarged; note that one encounters only supersonic solitary excitations.

In Fig. 6, we have numerically analyzed the Sagdeev potential [see Eq. (32) in Ref. 1] and investigated how the propagation speed λ, the positron-to-electron density ratio δ and the electron-to-ion temperature ratio σ_i change the profile of the potential well. Recall that only the region of negative values of $V(\phi)$ is physically relevant, and that the width of that region determines the maximum pulse amplitude, while its depth determines the slope (the spatial extension, essentially) of the pulse excitation. In Fig. 6a, an increase in the propagation speed λ leads to a decrease in both the potential width and depth (compare the solid to the dashed curves). In a similar manner, in Fig. 6b, by increasing δ (i.e. for less fixed ions in the background) one finds an increase in both potential width and depth. In Fig. 6c we see that, by increasing σ_i (i.e. for hotter electrons), both the potential width and depth decreases in the positive ϕ region (right horizontal semi-axis), while the inverse effect is seen to occur in the negative (left horizontal) semi-axis.

Figure 7 shows the dependence of the compressive and rarefactive potential pulse(s) on the propagation speed λ, the positron-to-electron density ratio δ and the electron-to-ion temperature ratio σ_i. It is obvious, from Fig. 7a, that faster solitary excitations are lower and narrower. We ought to stress again (cf. the discussion in Ref. 1) that this peculiar behavior is rather against the previous knowledge from the KdV theory, yet is an outcome of the algebraic transformations here; this implies no contradiction, as explained in Ref. 1). Increasing δ (i.e. for less background ions) leads to an increase in both pulse amplitude and width (see Fig. 7b). The positive (negative) solitary pulse amplitude and width decreases (increases) with increasing σ_i.

The paragraph following Eq. (41) in Ref. 1 contains a textual error. The correct sentence in the 3rd to 5th line(s) below Eq. (41) should read:
"However, negative values of both A and C are partially excluded, as we see in Figs. 3 - 5 [upon a simple comparison of parts (a) and (c) therein]."

In Figs. 8 and 9, we have numerically investigated the effects of the propagation speed λ, the positron-to-electron density ratio δ and the electron-to-ion temperature ratio σ_i on the behavior of the Sagdeev pseudo-potential (41) and the electrostatic potential (42) (of Ref. 1). We recall that the position of the double root determines the amplitude of resulting double-layer (DL) excitations, while the potential depth at the minimum here determines

the slope (and the width) of the excitation. It is found (see Figs. 8a and 9a) that increasing the velocity λ leads to a larger (taller, in amplitude) excitation. The DL amplitude is increased by increasing the positron concentration, i.e. for higher δ values (see Figs. 8b and 9b). Finally, an increase in the ionic temperature (i.e., smaller values of σ_i) shrinks the DL amplitude; in the limit $\sigma_i \to 0$ (fixed ion limit), no DL excitations are expected to occur.

The dependence of the double layer characteristics on the propagation speed λ, the electron-to-ion temperature ratio σ_i and the positron-to-electron density ratio δ is displayed in Fig. 9. It is seen (Fig. 9a) that both the amplitude and width of the double layers decrease for higher propagation speed. Increasing δ (Fig. 9b) leads to an increase in the amplitude (and the width, yet only slightly). In Fig. 9c, it is seen that the amplitude (width) increases (decreases) with the increase of σ_i.

The correct form of Fig. 10 is also presented (only quantitatively modified with respect to Ref. 1, yet same qualitative interpretation).

Finally, the paragraph below Eq. (44) in Ref. 1 should read:
"As we saw above, B is always positive, while the existence of double layer requires $C < 0$. It is also noted from Eq. (40) that the nature of the double layer depends on the sign of A, i.e. for $A > 0$ a positive double layer exists (viz $\varphi_m > 0$; see (40)), whereas for $A < 0$ we would have a negative double layer ($\varphi_m < 0$). The numerical analysis in Figs. 2-5 [see parts (a) and (c) therein] show that for high λ values the dominant situation corresponds to $C > 0$ and $A \sim \varepsilon$, so double layers cannot exist in that case. However, for small λ, double layers may occur, since $C < 0$ and $A \sim \varepsilon$. Furthermore, it is seen that for small λ, the nonlinear coefficient A has positive value and therefore only positive double layers can exist. However, for large values of δ, as in Fig. 5(a,c), it is clear that for λ near 4.2, $A \sim \varepsilon$ and $C < 0$, thus supersonic DLs can exist in this case."

Concluding, we regret having had to provide these amendments to Ref. 1, and do hope to have fulfilled our aim now, namely providing an efficient basis of reference for the modelling of nonlinear excitations in e-p-i plasmas in a cylindrical 2D geometry.

References

[1] W. M. Moslem, I. Kourakis, P. K. Shukla and R. Schlickeiser, Phys. Plasmas **14**, 102901 (2007).

Figure Captions

Figure 1.

(a) The soliton amplitude φ_0 is depicted against the propagation speed λ, for $\sigma_i = 1/300$, $\delta = 0.4$ (solid curve), $\delta = 0.9$ (dashed curve), and $\sigma_i = 1/3$ and $\delta = 0.4$ (dotted curve). (b) The soliton width W is depicted against λ for $\delta = 0.1$ (solid curve), $\delta = 0.5$ (dashed curve) and $\delta = 0.99$ (dotted curve). Here we have used $U_0 = 0.1$.

Figure 2.

The electrostatic potential $\varphi^{(1)}$ is depicted against the radial and angular coordinates, r and θ,respectively: (a) compressive solitary pulse for $\lambda = 1$ and (b) rarefactive solitary pulse for $\lambda = 2$. The other plasma parameters are $\sigma_i = 1/300$, $\delta = 0.4$, $U_0 = 0.1$ and $t = 1$.

Figure 3.

(a) The nonlinear coefficient A, (b) the determinant Δ [see (34) in Ref. 1], and (c) the nonlinear coefficient C are depicted against the propagation speed λ, for $\sigma_i = 1/3$ (solid curve), $\sigma_i = 1/300$ (dashed curve), where $\delta = 0.1$.

Figure 4.

(a) The nonlinear coefficient A, (b) the determinant Δ [see (34) in Ref. 1], and (c) the nonlinear coefficient C are depicted against the propagation speed λ, for $\sigma_i = 1/3$ (solid curve), $\sigma_i = 1/4$ (dashed curve), where $\delta = 0.5$.

Figure 5.

(a) The nonlinear coefficient A, (b) the determinant Δ , and (c) the nonlinear coefficient C are depicted against the propagation speed λ, for $\sigma_i = 1/3$ (solid curve), $\sigma_i = 1/300$ (dashed curve), where $\delta = 0.9$.

Figure 6.

The Sagdeev potential $V(\varphi^{(1)})$ is depicted against the electrostatic potential $\varphi^{(1)}$, for (a) $\sigma_i = 1/3$, $\delta = 0.1$, $\lambda = 2.45$ (solid curve), $\lambda = 2.55$ (dashed curve), (b) $\sigma_i = 1/3$, $\lambda = 2.45$, $\delta = 0.1$ (solid curve), $\delta = 0.11$ (dashed curve), (c) $\delta = 0.5$, $\lambda = 3.5$,$\sigma_i = 0.25$ (solid curve) and $\sigma_i = 0.24$ (dashed curve).

Figure 7.

The potential $\varphi^{(1)}$ [represented by Eqs. (35) and (36)] is depicted against χ for (a) $\sigma_i = 1/3$, $\delta = 0.1$, $\lambda = 2.45$ (solid curve), $\lambda = 2.5$ (dashed curve), (b) $\sigma_i = 1/3$, $\lambda = 2.45$, $\delta = 0.1$ (solid curve), $\delta = 0.11$ (dashed curve), (c) $\delta = 0.5$, $\lambda = 3.5$, $\sigma_i = 0.25$ (solid curve) and $\sigma_i = 0.24$ (dashed curve).

Figure 8.

The pseudo-potential $V(\varphi^{(1)})$ is depicted against the electrostatic potential $\varphi^{(1)}$, for (a) $\sigma_i = 1/3$, $\delta = 0.5$, $\lambda = 0.1$ (solid curve), $\lambda = 0.2$ (dashed curve), (b) $\sigma_i = 1/3$, $\lambda = 0.2$, $\delta = 0.3$ (solid curve), $\delta = 0.4$ (dashed curve), (c)$\delta = 0.6$, $\lambda = 0.2$, $\sigma_i = 1/3$ (solid curve) and $\sigma_i = 1/300$ (dashed curve).

Figure 9.

The double layer profile $\varphi^{(1)}$ [represented by Eq. (42)] is depicted against χ for (a) $\sigma_i = 1/3$, $\delta = 0.5$, $\lambda = 0.1$ (solid curve) and $\lambda = 0.2$ (dashed curve), (b) $\sigma_i = 1/3$, $\lambda = 0.2$, $\delta = 0.3$ (solid curve), $\delta = 0.4$ (dashed curve), (c) $\delta = 0.6$, $\lambda = 0.2$, $\sigma_i = 1/3$ (solid curve) and $\sigma_i = 1/300$ (dashed curve).

Figure 10.

The solitary pulse solutions [represented by Eqs. (35) and (36)] and the double layer profile [represented by Eq. (42)] are depicted against the radial and angular coordinates, r and θ,respectively: (a) compressive pulse, (b) rarefactive pulse (for $\lambda = 2.45$, $\sigma_i = 1/3$, $\delta = 0.1$, $U_0 = 0.1$ and $t = 1$, in both plots) and (c) double layer profile for $\lambda = 0.5, \sigma_i = 1/3$, $\delta = 0.5$, $U_0 = 0.1$ and $t = 1$.

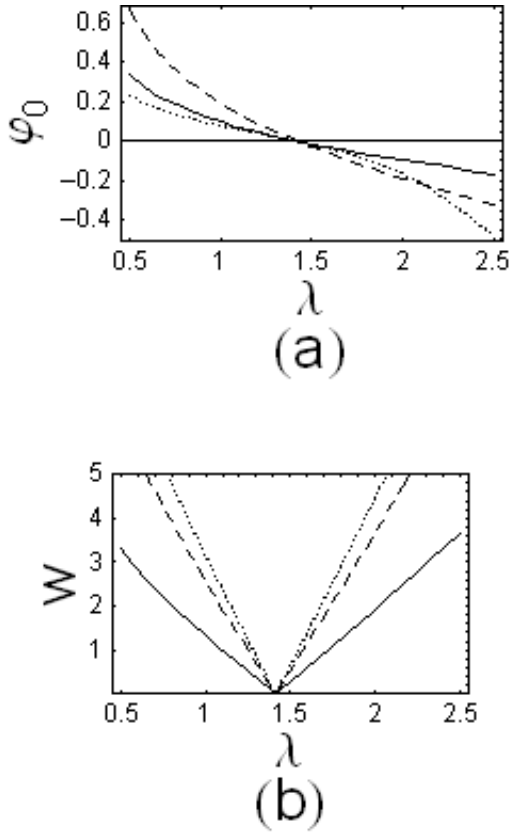
0.6
0.4
0.2
0
−0.2
−0.4
φ_0
0.5
1
1.5
2
2.5
λ
(a)
5
4
3
2
1
W
0.5
1
1.5
2
2.5
λ
(b)

Figure 1

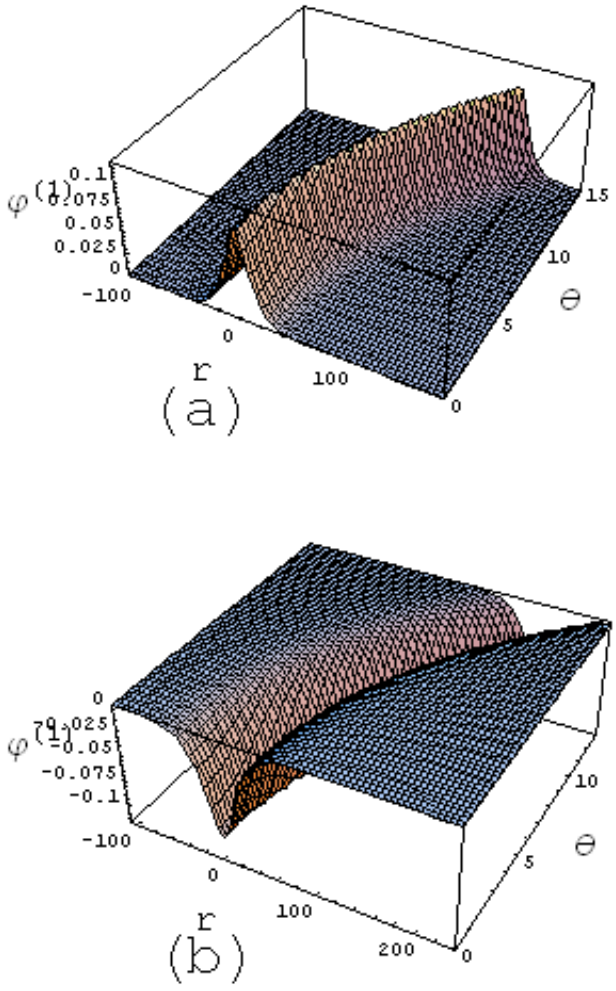
φ(1)
0.1
0.075
0.05
0.025
0
-100
0
100
r
(a)
0
5
10
15
Θ

φ(1)
0
-0.025
-0.05
-0.075
-0.1
-100
0
100
200
r
(b)
0
5
10
Θ

Fig 2

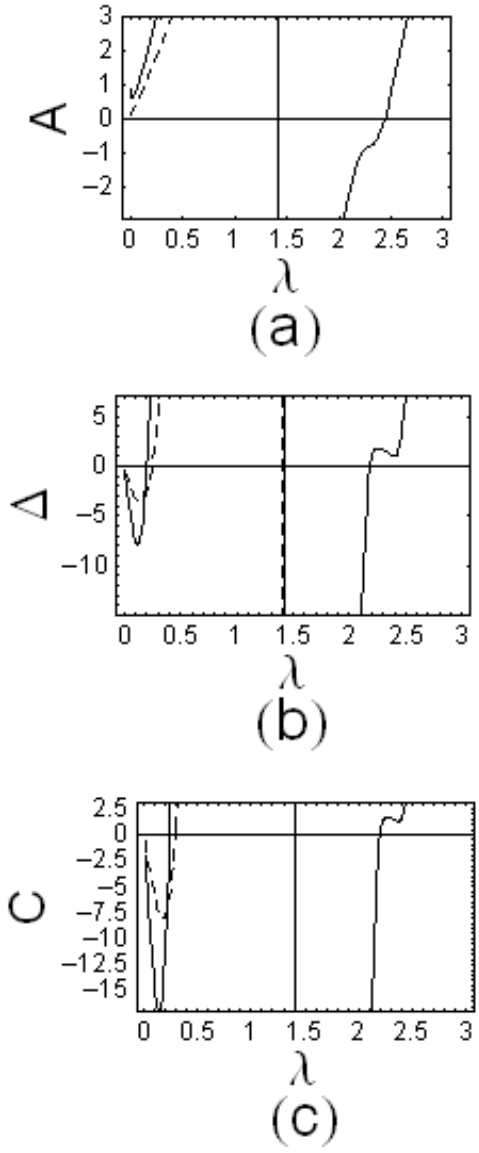

Fig 3

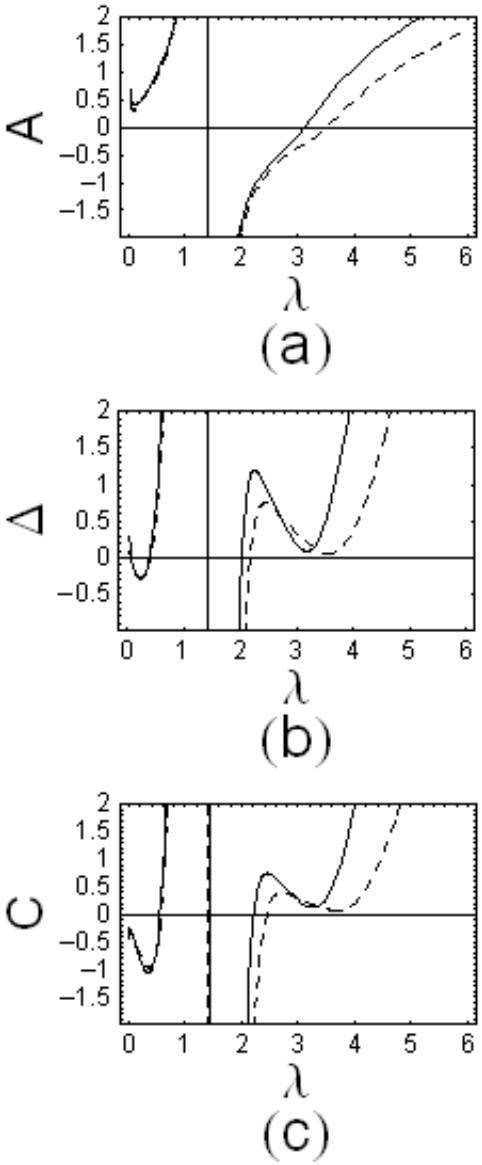

Fig 4

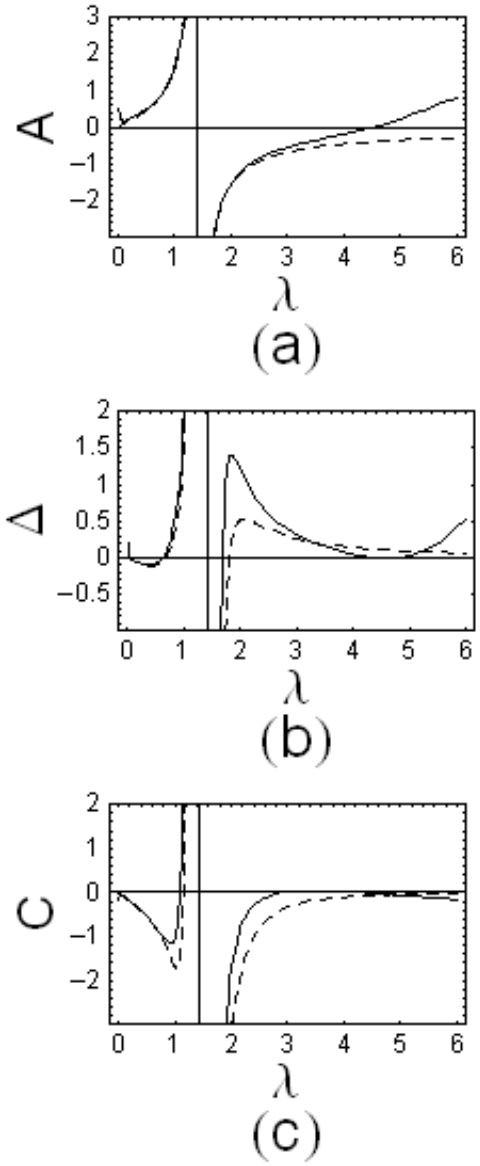

Fig 5

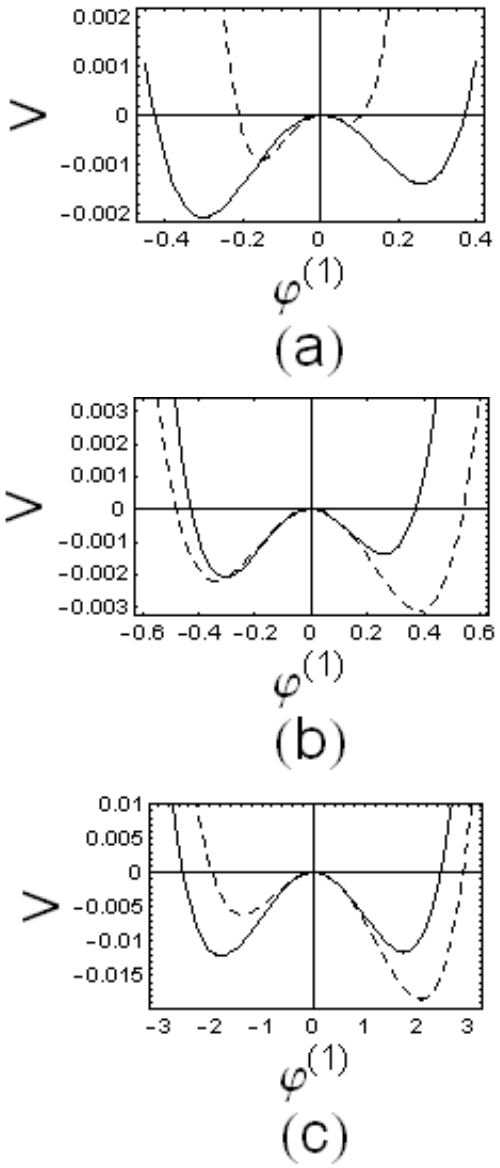
0.002
0.001
0
-0.001
-0.002
V
-0.4 -0.2 0 0.2 0.4
$\varphi^{(1)}$
(a)
0.003
0.002
0.001
0
-0.001
-0.002
-0.003
V
-0.6 -0.4 -0.2 0 0.2 0.4 0.6
$\varphi^{(1)}$
(b)
0.01
0.005
0
-0.005
-0.01
-0.015
V
-3 -2 -1 0 1 2 3
$\varphi^{(1)}$
(c)

Fig 6

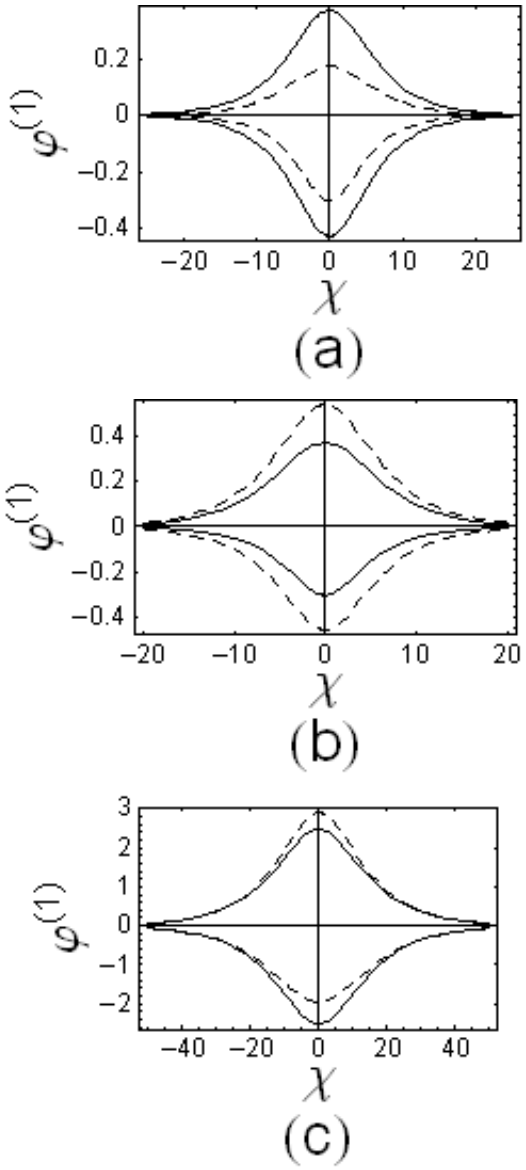
0.2
0
−0.2
−0.4
−20 −10 0 10 20
χ
(a)
0.4
0.2
0
−0.2
−0.4
−20 −10 0 10 20
χ
(b)
3
2
1
0
−1
−2
−40 −20 0 20 40
χ
(c)

Fig 7

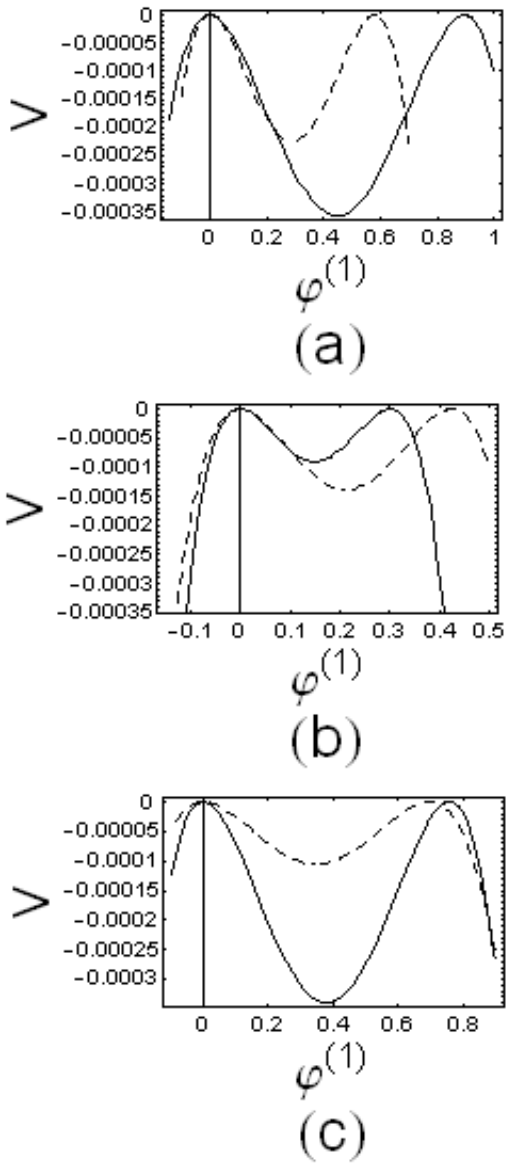
V
0
-0.00005
-0.0001
-0.00015
-0.0002
-0.00025
-0.0003
-0.00035
0 0.2 0.4 0.6 0.8 1
$\varphi^{(1)}$
(a)
V
0
-0.00005
-0.0001
-0.00015
-0.0002
-0.00025
-0.0003
-0.00035
-0.1 0 0.1 0.2 0.3 0.4 0.5
$\varphi^{(1)}$
(b)
V
0
-0.00005
-0.0001
-0.00015
-0.0002
-0.00025
-0.0003
0 0.2 0.4 0.6 0.8
$\varphi^{(1)}$
(c)

Fig 8

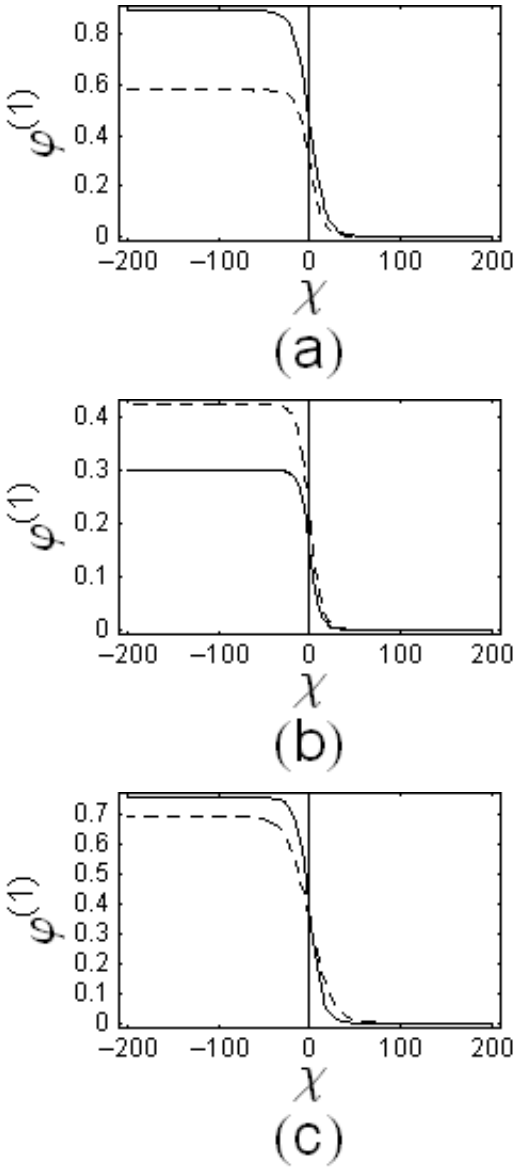
0.8
0.6
0.4
0.2
0
$\varphi^{(1)}$
−200 −100 0 100 200
χ
(a)
0.4
0.3
0.2
0.1
0
$\varphi^{(1)}$
−200 −100 0 100 200
χ
(b)
0.7
0.6
0.5
0.4
0.3
0.2
0.1
0
$\varphi^{(1)}$
−200 −100 0 100 200
χ
(c)

Fig 9

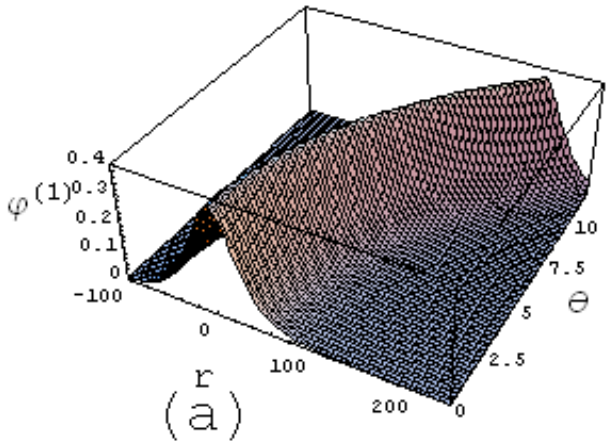
φ(1)
0.4
0.3
0.2
0.1
0
-100
0
100
200
r
0
2.5
5
7.5
10
θ
(a)

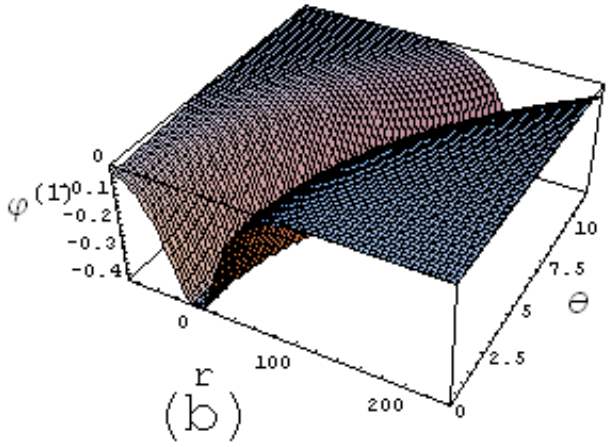
φ(1)
0
-0.1
-0.2
-0.3
-0.4
0
100
200
r
0
2.5
5
7.5
10
θ
(b)

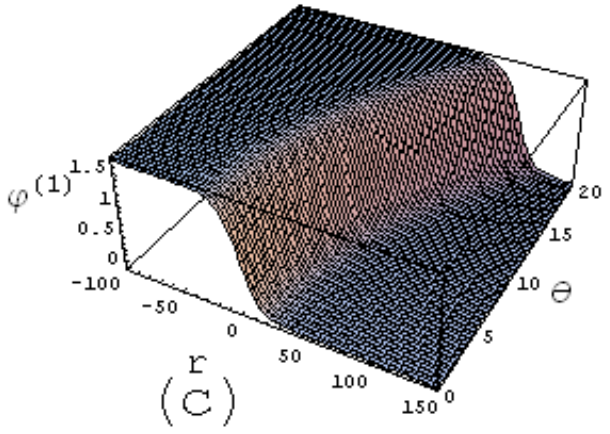
φ(1)
1.5
1
0.5
0
-100
-50
0
50
100
150
r
0
5
10
15
20
θ
(c)

Fig 10